Chiral phase transition at finite chemical potential in 2 + 1-flavor soft-wall anti–de Sitter space QCD

Sean P. Bartz[*] and Theodore Jacobson[†]

Department of Physics and Astronomy, Macalester College, St. Paul, Minnesota 55105, USA

The phase transition from hadronic matter to chirally symmetric quark-gluon plasma is expected to be a rapid crossover at zero quark chemical potential (μ), becoming first order at some finite value of μ, indicating the presence of a critical point. Using a three-flavor soft-wall model of anti–de Sitter/QCD, we investigate the effect of varying the light and strange quark masses on the order of the chiral phase transition. At zero quark chemical potential, we reproduce the Columbia Plot, which summarizes the results of lattice QCD and other holographic models. We then extend this holographic model to examine the effects of finite quark chemical potential. We find that the the chemical potential does not affect the critical line that separates first-order from rapid crossover transitions. This excludes the possibility of a critical point in this model, suggesting that a different setup is necessary to reproduce all the features of the QCD phase diagram.

I. INTRODUCTION

The investigation of the phase diagram for quark matter is a major project of nuclear physics. In particular, heavy-ion community is interested in mapping the phase transition between hadronic matter and the quark-gluon plasma as a function of temperature and baryon chemical potential. In particular, the search for the expected critical point in this phase boundary is the focus of the next run at the Relativistic Heavy Ion Collider (RHIC) at Brookhaven National Laboratory. A robust theoretical description of the phase boundary is thus a worthy goal.

Results from lattice QCD have demonstrated that the deconfinement phase transition at zero quark chemical potential (μ) is a rapid crossover. Extending lattice results to finite chemical potential is prevented by a well-known obstacle known as the sign problem. Techniques exist for extending lattice QCD to finite but relatively small values of μ, results which show no evidence of a critical point but place limits on its location [1–3].

Phenomenological models inspired by the anti–de Sitter/conformal field theory (AdS/CFT) correspondence [4–6] have succeeded in describing some aspects of the quark-gluon plasma [7,8]. Previous work has mapped the chiral phase transition as a function of temperature and quark chemical potential [9–14]. In two-flavor models, the phase transition is a crossover for zero quark mass and second order for nonzero quark mass. This is consistent with lattice QCD models, which

find the order of the order of the chiral phase transition to be dependent on the light and strange quark masses. Some holographic models have shown evidence of a critical point by examining baryon susceptibilities [15–18], but these models do not examine chiral symmetry restoration, which is the focus of this work.

The chiral phase structure for varying quark masses is summarized by the Columbia Plot [19,20], sketched in Fig. 1. Visualizing μ as a third axis of the Columbia Plot, the second-order line becomes a critical surface. To achieve the expected critical point in the $T-\mu$ plane, the critical surface should have the curvature shown in Fig. 2, with the physical point being in the crossover region at $\mu = 0$. The behavior of a pure gauge theory, found in the upper-right corner of the plot, is beyond the scope of this work.

Our previous work [9] examined light quarks only, corresponding to the $N_f = 2$ line of the Columbia Plot, where m_s is effectively infinite. In this regime, the chiral phase transition is a rapid crossover for finite quark mass and second-order for massless quarks. The authors of Ref. [21] studied the Columbia Plot at zero chemical potential in a soft-wall model of AdS/QCD. In this paper, we reproduce these results and extend this holographic analysis to finite chemical potential.

II. SOFT-WALL MODEL

To consider the thermodynamics of AdS/QCD, we use an asymptotically anti–de Sitter 5D black hole metric,

$$ds^2 = \frac{L^2}{z^2}\left[-f(z)dt^2 + dx_i^2 + \frac{dz^2}{f(z)}\right]. \qquad (1)$$

Following the procedure established in our previous work and in Refs. [22–24], we model finite temperature and chemical potential with a charged black hole described by the 5D

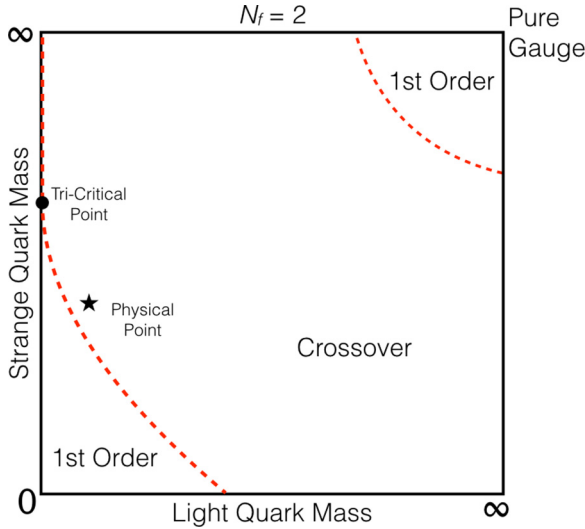*sbartz@macalester.edu
†tjacobs1@macalester.edu

FIG. 1. A sketch of the expected Columbia Plot, indicating the order of the chiral phase transition as a function of light and strange quark masses at zero chemical potential. The crossover region is separated from regions of first-order phase transitions by second-order phase transition lines.

FIG. 2. The critical surface separates first order from crossover phase transitions. Image taken from Ref. [20].

AdS–Reissner-Nordström metric

$$f(z) = 1 - (1 + Q^2)\left(\frac{z}{z_h}\right)^4 + Q^2\left(\frac{z}{z_h}\right)^6, \qquad (2)$$

where z_h is the location of the event horizon and $Q = q z_h^3$ is the black hole charge with the constraint $0 < Q^2 < 2$. The chemical potential and temperature are uniquely determined by the charge and horizon position

$$\mu = \kappa \frac{Q}{z_h}, \qquad (3)$$

$$T = \frac{1}{\pi z_h}\left(1 - \frac{Q^2}{2}\right). \qquad (4)$$

Note that μ is the quark chemical potential, with a value one third of the baryon chemical potential. As in Ref. [11] we take $\kappa = 1$.

The matter fields are described by the action

$$\mathcal{S} = \frac{1}{2k}\int d^5x \sqrt{-g}\, e^{-\Phi(z)}\,\mathrm{Tr}[|DX|^2 + V_m(X)], \qquad (5)$$

where X contains the scalar and pseudoscalar meson fields. We exclude the vector and axial-vector meson fields to focus on chiral dynamics. The dilaton field $\Phi(z)$ acts to smoothly cut off the action and introduce confinement in soft-wall AdS/QCD models. A quadratic IR dilaton $\Phi(z \to \infty) \sim z^2$ is required for linear confinement [6,25]. In order to dynamically solve for the chiral field, the dilaton must become negative quadratic in the
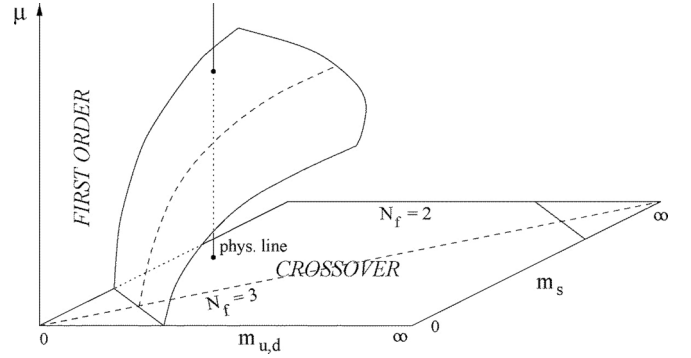
UV limit [12]. One example of a dilaton profile that produces good meson spectra in the zero-temperature limit [9] is

$$\Phi(z) = -\mu_1^2 z^2 + \left(\mu_0^2 + \mu_1^2\right)z^2\left[1 - \exp\left(-\mu_2^2 z^2\right)\right], \qquad (6)$$

with $\mu_0 = 430$ MeV, $\mu_1 = 830$ MeV, and $\mu_2 = 176$ MeV.

The vacuum expectation value (VEV) of the scalar field describes the chiral symmetry breaking of the model. In a two-flavor symmetric model, the VEV is given by

$$\langle X \rangle = \frac{\chi(z)}{2} I, \qquad (7)$$

where I is the $N_f \times N_f$ identity matrix. Allowing for flavor asymmetry, the scalar VEV takes the form

$$\langle X \rangle = \begin{pmatrix} \frac{\chi_l(z)}{\sqrt{2}} & 0 & 0 \\ 0 & \frac{\chi_l(z)}{\sqrt{2}} & 0 \\ 0 & 0 & \frac{\chi_s(z)}{\sqrt{2}} \end{pmatrix}, \qquad (8)$$

where the normalization factor is chosen to give the kinetic term its canonical form.

The features of this particular model are established by the choice of scalar potential $V_m(X)$. The AdS/CFT dictionary establishes the mass term, and a quartic term is necessary to obtain independent sources of explicit and spontaneous chiral symmetry breaking [6,26,27]. We also include t'Hooft determinant term in the scalar potential to introduce flavor mixing [12]. The potential becomes

$$V_m(X) = m_5^2|X|^2 + 4v_4|X|^4 + \gamma \mathrm{Re}[\det(X)], \qquad (9)$$

where $\gamma = 6\sqrt{2}\, v_3$. As before, we take $v_4 = 8$, and in the following set $v_3 = -3$.

III. CHIRAL SYMMETRY RESTORATION

To examine the chiral dynamics, we consider the behavior of the background chiral fields. The chiral potential is found to be

$$V(\chi) = \langle \mathrm{Tr}[V_m(X)] \rangle = m_5^2\left(\chi_l^2 + \tfrac{1}{2}\chi_s^2\right) + 3v_3\chi_l^2\chi_s + v_4\left(2\chi_l^4 + \chi_s^4\right). \qquad (10)$$
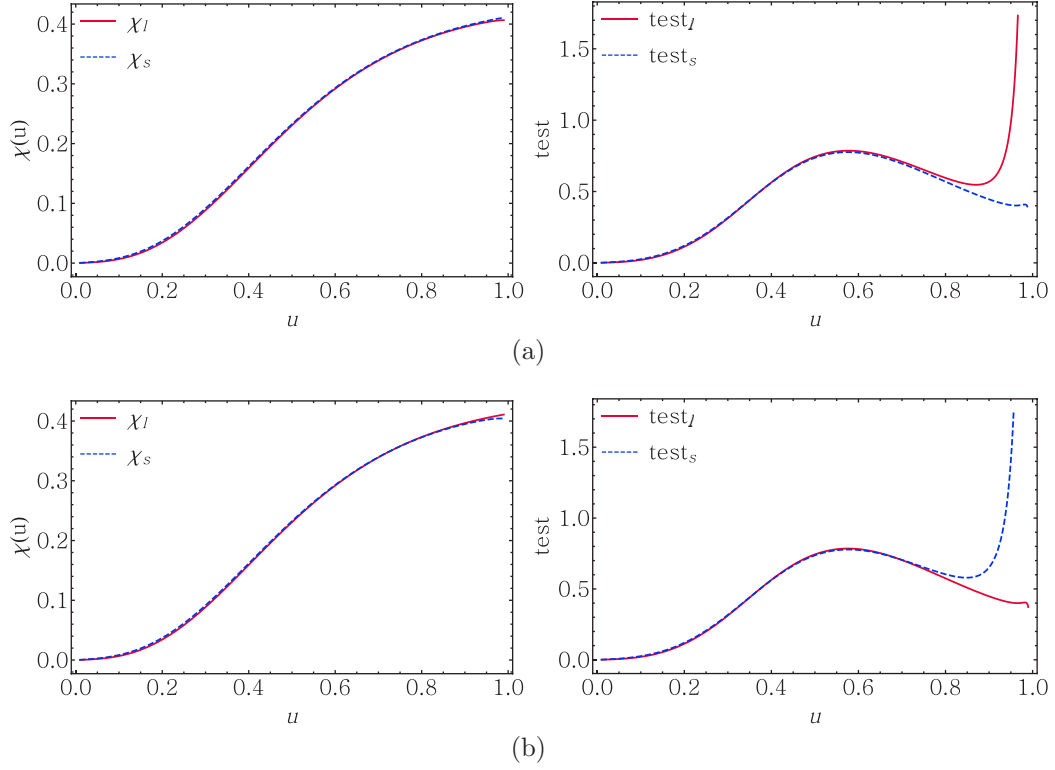
FIG. 3. Numerical solutions for the chiral fields and associated test functions, for the cases (a) $\sigma_l = (488.528 \text{ MeV})^3, \sigma_s = (482.004 \text{ MeV})^3$ and (b) $\sigma_l = (488.595 \text{ MeV})^3, \sigma_s = (482.010 \text{ MeV})^3$.

Varying the action (5) yields the equations of motion

$$\chi_l'' - \left[\frac{3f(u) - uf'(u) + uf(u)\Phi'(u)}{uf(u)}\right]\chi_l' + \frac{1}{u^2 f(u)}\left(3\chi_l - 3v_3\chi_l\chi_s - 4v_4\chi_l^3\right) = 0, \tag{11}$$

$$\chi_s'' - \left[\frac{3f(u) - uf'(u) + uf(u)\Phi'(u)}{uf(u)}\right]\chi_s' + \frac{1}{u^2 f(u)}\left(3\chi_s - 3v_3\chi_l^2 - 4v_4\chi_s^3\right) = 0, \tag{12}$$

where we have changed variables to $u = z/z_h$. The coupling of the light and strange sectors is evident and vanishes in the case $v_3 = 0$. The UV boundary conditions on the chiral fields are determined by the AdS/CFT dictionary

$$\chi_l(u \to 0) = m_l\zeta z_h u + \frac{\sigma_l}{\zeta}z_h^3 u^3, \quad \chi_s(u \to 0)$$

$$= m_s\zeta z_h u + \frac{\sigma_s}{\zeta}z_h^3 u^3, \tag{13}$$

where $m_l = m_{u,d}$ is the light quark mass and m_s is the strange quark mass, and there are two chiral condensates $\sigma_l = \langle \bar{u}u \rangle = \langle \bar{d}d \rangle$ and $\sigma_s = \langle \bar{s}s \rangle$. The normalization $\zeta = \sqrt{N_c}/(2\pi)$ is determined from large-N QCD [28]. For a given quark mass, we solve for the chiral condensates as a function of temperature and baryon density. Previous work shows that the T and μ dependence of the phase transition is qualitatively equivalent [9]. For clarity of illustration, we will plot σ_l, σ_s as functions of temperature only.

A. Numerical shooting method

The chiral condensates σ_l and σ_s are determined by numerically solving the boundary value problem (11) and (12), subject to the UV boundary condition (13) and the near-horizon condition that the chiral fields are regular.

Using the shooting method converts a the boundary value problem into an initial value problem, and we vary σ_l, σ_s until we find a combination that satisfies the near-horizon condition. Integrating closer to the singular points at $u = 0, 1$ increases the sensitivity of the method, and for this analysis we let u range from 10^{-2} to $1-10^{-2}$. Because it is difficult to determine when the chiral fields χ_l, χ_s are regular, we isolate the singular parts of the equations of motion,

$$\text{test}_l = u^2\frac{f'}{f} + \frac{1}{f}\left(3\chi_l - 3v_3\chi_l\chi_s - 4v_4\chi_l^3\right), \tag{14}$$

$$\text{test}_s = u^2\frac{f'}{f} + \frac{1}{f}\left(3\chi_s - 3v_3\chi_l^2 - 4v_4\chi_s^3\right), \tag{15}$$

and analyze their near-horizon behavior to determine the existence of a regular solution.
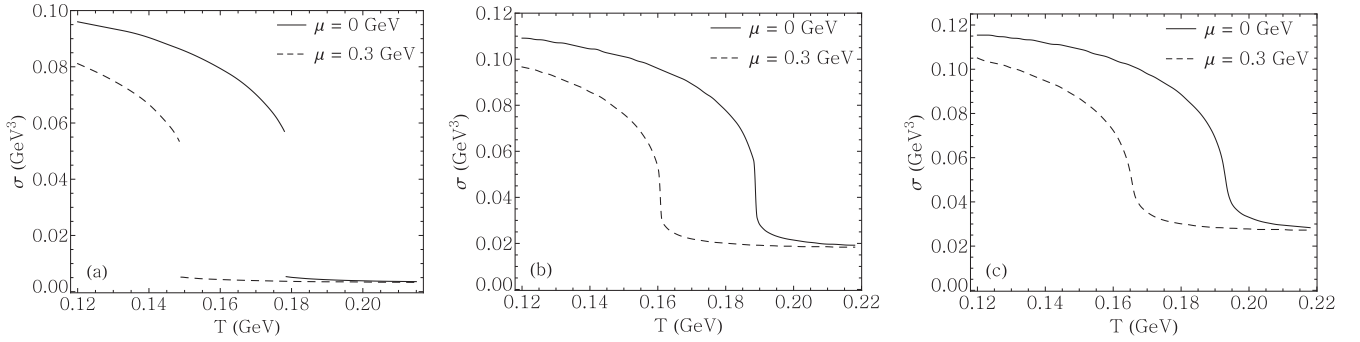
FIG. 4. Dependence of σ on T for zero and nonzero values of μ and (a) $m_l = m_s = 10$ MeV, (b) $m_l = m_s = 35$ MeV, and (c) $m_l = m_s = 45$ MeV. In all cases, chemical potential has no effect on the order of the phase transition.

We show a representative case for $\mu = 0$, $T = 140$ MeV, $m_l = 40$ MeV, and $m_s = 70$ MeV. Figure 3 shows that when $\sigma_l = (488.528 \text{ MeV})^3$ and $\sigma_s = (482.004 \text{ MeV})^3$, test$_s$ is regular as it approaches the horizon while test$_l$ diverges to positive infinity. When the shooting parameters are altered slightly to $\sigma_l = (488.595 \text{ MeV})^3$ and $\sigma_s = (482.010 \text{ MeV})^3$, the behavior of the test functions reverses. This signals that there is a regular solution for both chiral fields in this region of parameter space. It is important to note that although the qualitative difference in the test functions is clear, the corresponding change in σ_l (respectively, σ_s) is 0.04% (respectively, 0.004%) and is indistinguishable in Fig. 3.

B. Flavor-symmetric case

We begin our analysis with the flavor-symmetric case. This is represented by the dashed line $m_l = m_s$ on the Columbia Plot. In this case, $\chi_l = \chi_s$, reducing (11) and (12) to the single equation of motion

$$\chi'' - \left[\frac{3f(u) - uf'(u) + uf(u)\Phi'(u)}{uf(u)} \right]\chi'$$
$$+ \frac{1}{u^2 f(u)}(3\chi - 3v_3\chi^2 - 4v_4\chi^3) = 0, \quad (16)$$

subject to the UV boundary condition (13). Using a numerical shooting method, we find the value of σ that produces solutions to (16) that are regular at the black hole horizon. When nontrivial solutions exist, they are energetically favored over the trivial solution $\chi(u) = 0$ [12]. Chiral symmetry restoration is realized at values of T, μ where nontrivial regular solutions do not exist, making the trivial solution the only solution and signifying $\sigma = 0$.

Although this version of the model is flavor symmetric, it does not simply mimic the two-flavor results of Ref. [9], which represent the top line of the Columbia Plot, where m_s is effectively infinite. The inclusion of the cubic t'Hooft determinant term in the scalar potential breaks the $\chi \leftrightarrow -\chi$ symmetry, giving energetic preference to positive chiral fields [12]. As a result, the $\sigma \leftrightarrow -\sigma$ symmetry found in the two-flavor case is also broken, allowing first-order phase transitions for some values of the quark mass.

The order of the phase transition is determined by the way in which the order parameters σ goes to zero. In a first-order transition, the order parameter is discontinuous at the critical temperature or chemical potential. In a second-order transition, the order parameter is continuous, but there is a discontinuity in its first derivative. A rapid crossover transition is characterized by an order parameter that is both continuous and smooth.
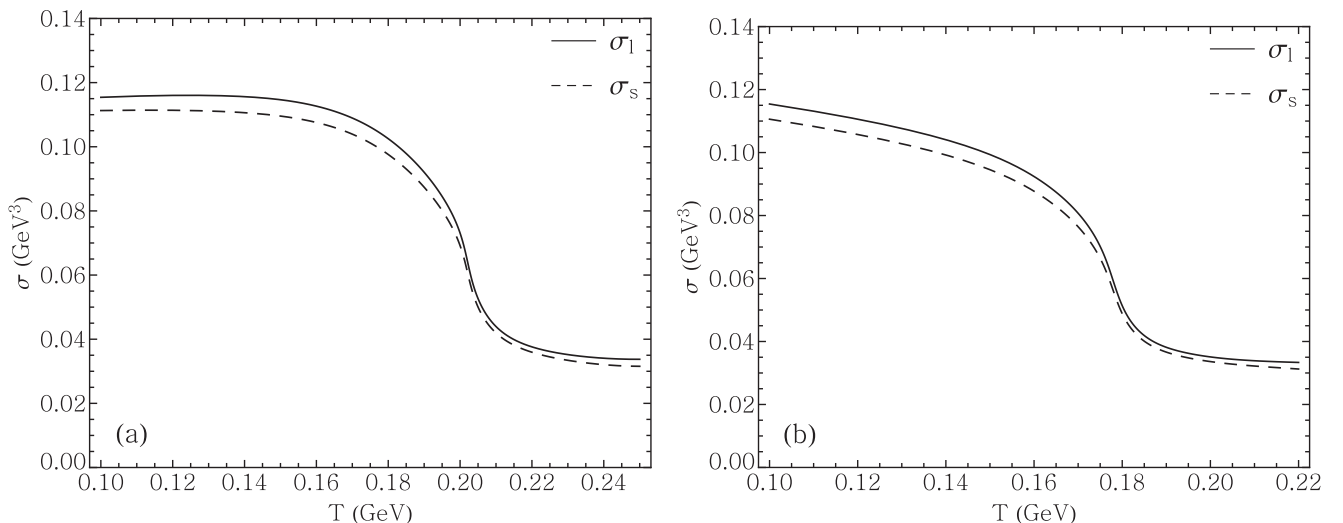

FIG. 5. Dependence of σ_l and σ_s on T with $m_l = 40$ MeV, $m_s = 70$ MeV and (a) $\mu = 0$ MeV and (b) $\mu = 300$ MeV.
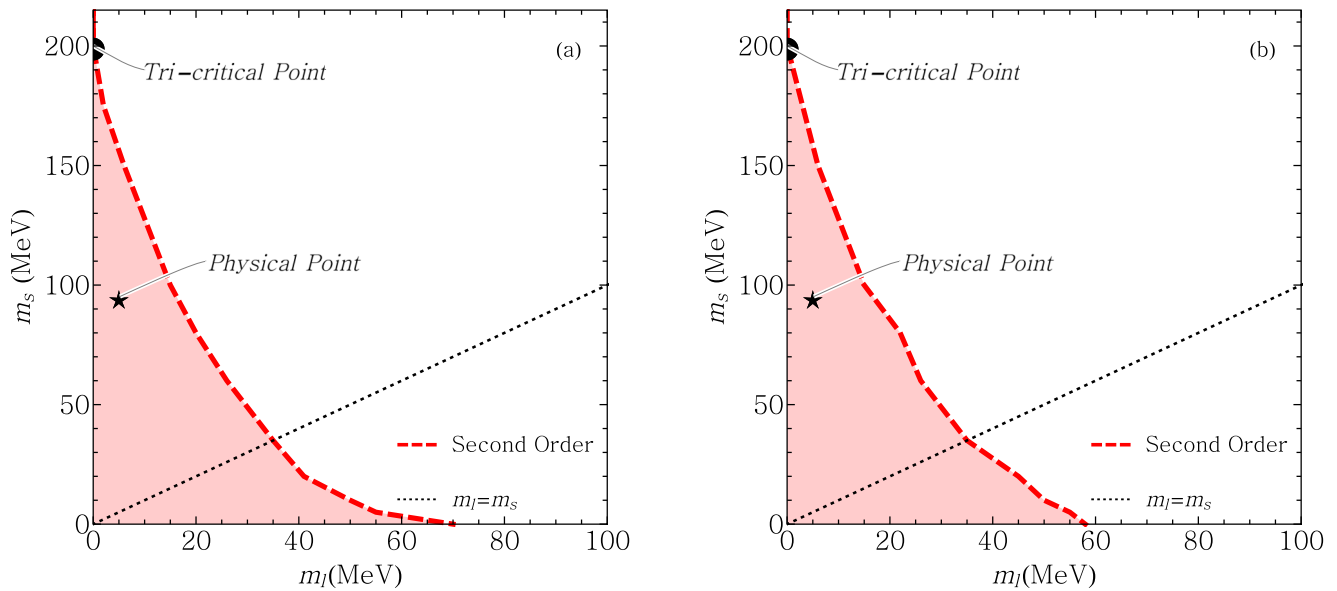
FIG. 6. The Columbia Plot for (a) $\mu = 0$ MeV and (b) $\mu = 300$ MeV. The shaded region indicates mass values where a first-order phase transition is produced, and the dashed line shows the line of second-order phase transitions separating it from the crossover region. The dotted line indicates the line of $m_s = m_l$.

The critical value of the quark mass separating first-order and crossover phase transitions is $m_q = 35$ MeV. Figure 4 shows examples of first-order, second-order, and crossover transitions for representative values of the quark mass and chemical potential. This critical quark mass is found to be independent of μ, implying that this flavor-symmetric model cannot produce a critical point in the $T-\mu$ plane.

C. 2 + 1-flavors

Finding no critical point in the flavor-symmetric case, we extend the model to $2 + 1$ flavors. The shooting is extended to find values of σ_l and σ_s that yield regular solutions for both chiral fields. Figure 5 shows a representative case for $m_l = 40$ MeV, $m_s = 70$ MeV at $\mu = 0$ MeV, and $\mu = 300$ MeV. As in the flavor-symmetric case, the order of the phase transition is not affected by the chemical potential. From Fig. 5 it is clear that σ_l and σ_s differ. In fact, by examining the case where $m_l = 0$ MeV, $m_s = 200$ MeV, we find that σ_l undergoes a second-order transition while the phase transition for σ_s is first order. In the case that the orders do not agree, we characterize the transition by the higher-order transition of the two order parameters.

The chiral phase structure at a particluar μ is summarized by finding the second-order line in the Columbia Plot. Figure 6 shows representative Columbia Plots for $\mu = 0$ and $\mu = 300$ MeV. We find the tricritical point, marking the end of the first-order region, at $m_s = 200$ MeV. At greater m_s values, second-order transitions occur at $m_l = 0$ and rapid crossover transitions occur for finite values. The physical point $m_l = 5$ MeV, $m_s = 95$ MeV is within the first-order region, contradicting expectations from lattice results at $\mu = 0$. The location of the second-order line may be adjusted by the choice of input parameters, but this work is focused on the dependence of the phase transition order on chemical potential.

At small m_s there are deviations in the second-order line on the order of 1 MeV as μ is varied. However, these small changes are likely numerical artifacts rather than evidence of a qualitative change. Thus, the phase transition order is unaffected by μ, indicating that the critical surface depicted in Fig. 2 has zero curvature in this model, and no critical point in the $T-\mu$ plane is possible.
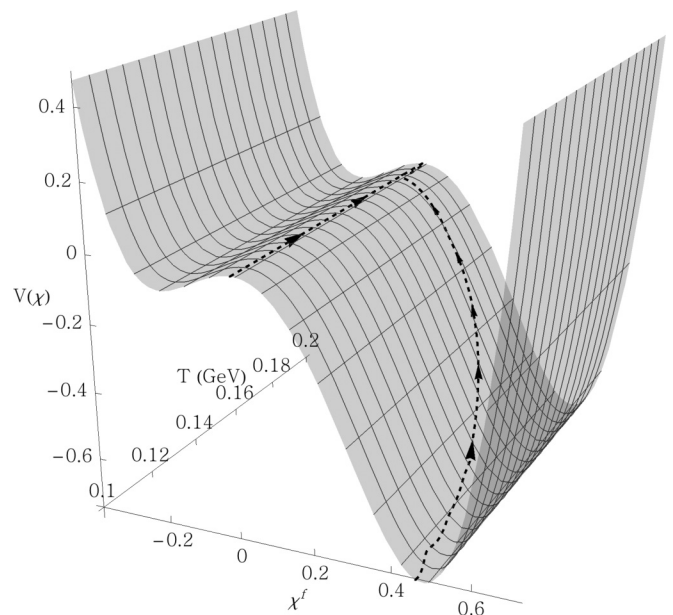

FIG. 7. Projection of χ^f onto $V(\chi)$ as a function of temperature for the case $m_l = m_s = 10$ MeV and $\mu = 0.010$ GeV. Symmetry restoration is clear at $T_c \sim 0.185$ GeV.
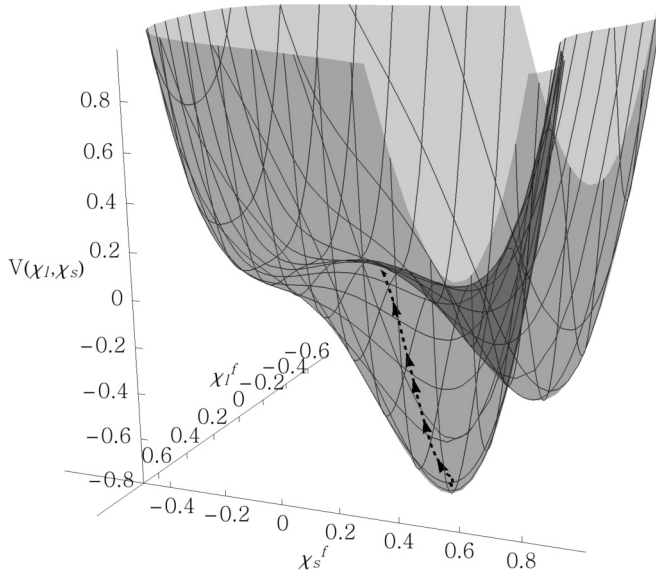
FIG. 8. Projection of χ_l^f and χ_s^f onto the surface of $V(\chi_l, \chi_s)$, parameterized by temperature in the range $T = [0.1, 0.23]$ GeV.

D. Chiral potential

Further analysis reveals how the solutions to (16) relate to the flavor-symmetric scalar potential (10). In particular, the effects of spontaneous symmetry breaking is evident from the vacuum states of potential. We examine $V(\chi^f)$, where $\chi^f \equiv \chi(u \to 1)$ is the near-horizon value of the chiral field. Figure 7 shows the temperature-independent potential for a representative case with $m_l = m_s = 10$ MeV and $\mu = 10$ MeV. The near-horizon solution is projected onto the potential, showing first-order chiral symmetry restoration as $T \to T_c$. The trivial solution $\chi(u) = 0$ is also plotted, but below $T = T_c$ it is energetically disfavored. Because m_q is small, the effects of explicit symmetry breaking are small, and at $\chi^f = 0$, chiral symmetry is restored. The potential is asymmetric in χ^f, in contrast to the two-flavor model which also permits negative solutions for χ, σ.

We perform a similar analysis for the $2 + 1$-flavor potential (10). With three flavors, we now project the temperature dependence of χ_l^f and χ_s^f onto the surface given by $V(\chi_l, \chi_s)$.

Figure 8 shows a representative case with $m_l = 30$ MeV, $m_s = 100$ MeV, and $\mu = 0.1$ GeV. The path along the surface is parameterized by temperature, ranging from 0.1 GeV to 0.23 GeV. The transition is crossover and the chiral fields do not vanish, a result of explicit chiral symmetry breaking due to the nonzero quark masses. As in the two-flavor case, when $T \to T_c$ the effects of spontaneous symmetry breaking disappear.

IV. CONCLUSION

In this work, we investigate the chiral phase transition in $2 + 1$-flavor soft-wall AdS/QCD at finite temperature and quark chemical potential. The scalar VEV is modified to include strange quarks and higher-order terms in the scalar potential are included in the action. A quartic term allows for independent sources of explicit and spontaneous chiral symmetry breaking, while a cubic t'Hooft determinant term allows for flavor mixing and first-order phase transitions. All analysis is performed in the finite chemical potential regime, using the AdS–Reissner-Nordström metric. Using the shooting method we numerically solve for the chiral field and extract the dependence of the chiral condensates on temperature and chemical potential.

In the flavor-symmetric case where $m_l = m_s$, we find critical quark mass $m_c = 35$ MeV separates first-order from crossover transitions. In agreement with lattice results and other nonperturbative methods, we find the second-order curve that separates first-order from crossover transitions for the flavor asymmetric case. When m_s is above the tricritical point, the results are consistent with the two flavor model, where the transition is second order at $m_l = 0$ and crossover otherwise.

This paper presents improvements on earlier results by incorporating finite chemical potential in a $2 + 1$-flavor model, enabling exploration of the full chiral dynamics. Because the this holographic model admits no critical point in the $T - \mu$ plane. Future work in this area should provide qualitative differences at finite quark chemical potential. One possibility is to couple quark chemical potential to the light quarks only. A modified black hole metric may also introduce qualitative differences between the effects of temperature and chemical potential. Finally, for a self-consistent model, the dilaton and black hole metric should be solved dynamically from the gravity action rather than being parameterized by hand.

[1] P. de Forcrand and O. Philipsen, J. High Energy Phys. 01 (2007) 077.

[2] C. Bonati, P. de Forcrand, M. D'Elia, O. Philipsen, and F. Sanfilippo, Phys. Rev. D **90**, 074030 (2014).

[3] R. Bellwied, S. Borsányi, Z. Fodor, J. Günther, S. D. Katz, A. Pásztor, C. Ratti, and K. K. Szabó, Nucl. Phys. A **956**, 797 (2016).

[4] J. Maldacena, Adv. Theor. Math. Phys. **2**, 231 (1998).

[5] E. Witten, Adv. Theor. Math. Phys. **2**, 505 (1998).

[6] A. Karch, E. Katz, D. T. Son, and M. A. Stephanov, Phys. Rev. D **74**, 015005 (2006).

[7] A. Vega and A. Ibañez, Eur. Phys. J. A **53**, 217 (2017).

[8] R. Zöllner and B. Kämpfer, Eur. Phys. J. A **53**, 139 (2017).

[9] S. P. Bartz and T. Jacobson, Phys. Rev. D **94**, 075022 (2016).

[10] L. X. Cui and Y. L. Wu, Mod. Phys. Lett. A **28**, 1350132 (2013).

[11] P. Colangelo, F. Giannuzzi, S. Nicotri, and V. Tangorra, Eur. Phys. J. C **72**, 2096 (2012).

[12] K. Chelabi, Z. Fang, M. Huang, D. Li, and Y.-L. Wu, J. High Energy Phys. 04 (2016) 036.

[13] Z. Fang, S. He, and D. Li, Nucl. Phys. B **907**, 187 (2016).

[14] Z. Fang, Y. Wu, and L. Zhang, Phys. Lett. B **762**, 86 (2016).

[15] R. Critelli, J. Noronha, J. Noronha-Hostler, I. Portillo, C. Ratti, and R. Rougemont, Phys. Rev. D **96**, 096026 (2017).

[16] R. Critelli, R. Rougemont, and J. Noronha, J. High Energy Phys. 12 (2017) 029.

[17] J. Knaute, R. Yaresko, and B. Kämpfer, Phys. Lett. B **778**, 419 (2018).

[18] Z. Li, Y. Chen, D. Li, and M. Huang, Chin. Phys. C **42**, 013103 (2018).

[19] F. R. Brown, F. P. Butler, H. Chen, N. H. Christ, Z. Dong, W. Schaffer, L. I. Unger, and A. Vaccarino, Phys. Rev. Lett. **65**, 2491 (1990).

[20] E. Laermann and O. Philipsen, Ann. Rev. Nucl. Part. Sci. **53**, 163 (2003).

[21] D. Li and M. Huang, J. High Energy Phys. 02 (2017) 042.

[22] A. Chamblin, R. Emparan, C. V. Johnson, and R. C. Myers, Phys. Rev. D **60**, 064018 (1999).

[23] C. Park, Phys. Rev. D **81**, 045009 (2010).

[24] P. Colangelo, F. Giannuzzi, and S. Nicotri, Phys. Rev. D **83**, 035015 (2011).

[25] A. Karch, E. Katz, D. T. Son, and M. A. Stephanov, J. High Energy Phys. 04 (2011) 066.

[26] T. Gherghetta, J. I. Kapusta, and T. M. Kelley, Phys. Rev. D **79**, 076003 (2009).

[27] S. P. Bartz and J. I. Kapusta, Phys. Rev. D **90**, 074034 (2014).

[28] A. Cherman, T. D. Cohen, and E. S. Werbos, Phys. Rev. C **79**, 045203 (2009).